The influence of hydrogen on cyclic plasticity of oriented nickel single crystal. Part I: Dislocation organisations and internal stresses

G. Hachet, A. Oudriss, A. Barnoush, R. Milet, D. Wan, A. Metsue, X. Feaugas

Version of Record: https://www.sciencedirect.com/science/article/pii/S0749641919304905
Manuscript_a4c4f98f3aec23e06515ac7be8b83c7e

The influence of hydrogen on cyclic plasticity of <001> oriented nickel single crystal. Part I: dislocation organisations and internal stresses.

G.Hachet[1,*], A.Oudriss[1], A.Barnoush[2], R.Milet[1], D.Wan[2], A.Metsue[1] and X.Feaugas[1]

[1]La Rochelle University, LaSIE UMR CNRS 7356, Avenue Michel Crépeau, 17000 La Rochelle.
[2]Department of Mechanical and Industrial Engineering, NTNU Richard Birkelands vei 2b, 7491, Trondheim, Norway
[*]Corresponding author: guillaume.hachet@gmx.com

Abstract: The present paper discussed the impact of hydrogen on the mechanical response of cyclically strained nickel single crystal oriented for multi-slips at different length scales. At macroscale, as a function of the plastic strain, the hydrogen seems to induce competition between softening and hardening of the metal. Then, by separating internal stresses induced by long-range and short-range interactions between dislocations (represented by back and effective stresses, respectively), we noted that hydrogen reduces the effective stress but has a more complex behaviour with the back stress. Therefore, observations with transmission electron microscope and nano-indentation tests have been performed on cyclically pre-strained nickel single crystal with and without hydrogen. The dislocation organisation induced by the cyclic tests is similar for nickel with and without hydrogen. In both cases, the dislocation arrangement can be affiliated to a composite structure with a wall phase containing mainly edge dislocation dipoles and a channel structure where the mobility and cross-slip events of screw dislocations occurred. From both approaches, we observed that hydrogen hardens the wall phase while it softens the channel phase. These results are discussed on the base of plasticity mechanisms.

Keywords: A: fatigue; B: crystal plasticity; C: mechanical testing; C: electron microscopy; hydrogen

1. Introduction

It is well-known that hydrogen affects the mechanical properties of metals inducing the premature failure of engineering structures under static or cyclic loadings (Blanc and Aubert, 2019; Gangloff and Somerday, 2011). From the damaged surfaces of the different structures, several models have been proposed to describe hydrogen embrittlement (HE) and have been reviewed in the non comprehensive literature (Ashby and Hirth, 1986; Barnoush and Vehoff, 2010; Feaugas and Delafosse, 2019; Hirth, 1980; Lynch, 2019, 2011; Magnin, 1995; Martin et al., 2019; Nagumo, 2016; Roberston et al., 2009; Robertson et al., 2015). In the work of Kirchheim (Kirchheim, 2007a, 2007b) as well as in a more recent review of Feaugas and Delafosse (Feaugas and Delafosse, 2019), this phenomenon is presented as the reduction of the energy to form or emit defects such as dislocations, vacancies, vacancy clusters… (Beachem, 1972; Birnbaum and Sofronis, 1994; Carr and McLellan, 2004; Delafosse and Magnin, 2001; dos Santos et al., 2003; Fukai, 2005; Hachet et al., 2018; Li et al., 2017), or the cohesive and surface energies (Kirchheim et al., 2015; Lynch, 1979; Oriani, 1970; Troiano, 1960). These different models encompass the interactions between hydrogen and defects, which have been unified in the work of Kirchheim (Kirchheim, 2007b, 2007a), through the use of "defactants" concept. However, the description of HE in metals becomes more delicate in case of plastically strained metals, which implicates to manage a large variety of length and time scales of several mechanisms.

Information on the impact of hydrogen on the mechanical response of tensile strained nickel is also available in the literature for single crystal oriented for single slip (load axis parallel to [135]) (Delafosse, 2012; Girardin et al., 2015; Girardin and Delafosse, 2004; Windle and Smith,

1968), nickel single crystal oriented for multi-slips (Ghermaoui et al., 2019; Girardin et al., 2015; Windle and Smith, 1968) and polycrystal (Boniszewski and Smith, 1963; Eastman et al., 1982; Harris et al., 2018; Kimura and Birnbaum, 1987; Lawrence et al., 2017; McInteer et al., 1980; Sirois and Birnbaum, 1992; Wang et al., 2017; Wilcox and Smith, 1964). When the metal is oriented for single slip, a clear competition between softening and hardening effect of hydrogen has been highlighted depending on the plastic strain (Girardin et al., 2015). The authors managed to explain the different mechanisms by investigating at lower length scales the induced dislocation structures with and without hydrogen. At low plastic strain, hydrogen in the Cottrell atmosphere increases the drag stress of edge dislocation and provokes a hardening. This effect has been also illustrated using discrete dislocation dynamics in nickel (Gu and El-Awady, 2018) and has been evaluated with a dynamics strain ageing study (Girardin and Delafosse, 2004). At larger plastic strain, the solute induces a shielding effect of dislocations and then increases the number of dislocations' sources, which softens the metal and supports the HELP (Hydrogen-Enhanced Localized Plasticity) model detailed in previous studies (Beachem, 1972; Birnbaum and Sofronis, 1994; Delafosse and Magnin, 2001). Then, at even larger plastic strain, the solute reduces the inter-wall dislocation structure, which has been observed with transmission electron microscopy (TEM). It induces the second hardening, which has been confirmed in a more recent study on polycrystalline nickel (Wang et al., 2017) and on single crystal oriented for multi-slips (Ghermaoui et al., 2019). Consequently, when the metal is tensile strained with and without hydrogen, the results at macroscale are deduced from the interactions between the solute and dislocations (and also dislocation pattern) visible at the microscale. To investigate these interactions and the consequences to the HE processes, *in-situ* electrochemical nano-indentation (ECNI) in nickel single crystal has been used previously in the literature. Such a technique allows evaluating the consequences of the solute for the onset of plasticity (Barnoush and Vehoff, 2010, 2008). The main result shows that hydrogen reduces the required stress for homogeneous dislocation nucleation through a combination of different phenomenological proposed model (Barnoush and Vehoff, 2010). This result has been also obtained with large-scale molecular dynamics (MD) simulations but to a limited extent, in the context of a quasi-homogeneous dislocations population (Zhou et al., 2016).

The impact of hydrogen on cyclically strained nickel single crystal has been less extensively studied than for tensile tests (Castelluccio et al., 2018; Magnin et al., 2001). It is well-known that cyclic loadings promote the formation of dipolar dislocation pattern in nickel single crystal as any FCC metals and alloys. From the evolution of the saturation stress with the plastic strain amplitude, different pre-dominant dislocations organisations have been related (Argon, 1996; Laird, 1996; P. Li et al., 2011; Mughrabi, 1978), which are similar for all face centred cubic (FCC) metal. They correspond to different cyclic hardening stages, which have been classified in the literature in the form of fatigue mechanisms maps (Feaugas and Pilvin, 2009; Pedersen, 1990). When single slip oriented FCC are cyclically strained, three hardening stages (II_0, III_0, III) have been observed (Feaugas and Pilvin, 2009; Li et al., 2009; P. Li et al., 2011; Mughrabi, 1978). The dislocation organisation is mainly separated into two phases, which are called wall structure containing mostly edge dislocation dipoles and channel structure where the mobility and cross-slip processes of screw dislocations occurred (Mughrabi, 1988, 1987, 1983). A previous study has been performed on the impact of hydrogen on the mechanical response of single slip oriented nickel single crystal (load axis parallel to [153]) (Magnin et al., 2001). The solute delays the beginning of stage III_0, which implicates a decrease of the cross-slip probability (Delafosse, 2012) and has been confirmed through numerical simulations (Gu and El-Awady, 2018; Wen et al., 2007). In addition, hydrogen reduces the saturated stress and softens the metal for all plastic strain amplitudes. This softening effect has been affiliated to a reduction of the internal shear in the persistent slip band (PSB), assuming hydrogen mainly segregated in wall dislocations structures. However, we still have limited information on the dislocation organisation induced by fatigue in nickel single crystal in the presence of hydrogen, the observed softening effect of hydrogen is obtained only for one hydrogen concentration and finally, the impact of hydrogen on the mechanical response of multi-slips oriented

nickel single crystal still remains unknown. Therefore, we propose this multi-scale study on the consequences of hydrogen on the mechanical responses of cyclically strained nickel single crystal oriented for multi-slips (load axis parallel to <001>) composed of two articles (part I and part II). The aim of this article (part I) is to evaluate experimentally the softening or/and hardening effect of hydrogen when nickel is cyclically strained, correlated it with the internal stresses and the dislocation structures induced by fatigue. The second part of this work (companion paper, part II) will focus on the understanding of the interactions between hydrogen and the fatigue-induced defects using a numerical approach.

2. Materials and method

2.1 Hydrogen incorporation and uniaxial cyclic tests

The study has been performed on nickel single crystals with a purity of 99.999% provided by Goodfellow. The specimens have been manufactured by the STEEC Company using the electro-erosion method (Oudriss et al., 2012). Hydrogen has been charged using two methods, which were electrochemical and chemical ways in a double-walled cell. The experimental procedure for the electrochemical way consisted in imposing a cathodic polarisation of -10mA/cm^2 in a 0.1M NaOH deaerated solution on both sides of the (100) crystallographic plane for 72 hours at 298K (Li et al., 2017; Oudriss, 2012). The thickness of the sample was 1 mm and the temperature has been kept constant during hydrogen charging by a thermocryostast. The concentrations of hydrogen measured with thermo-desorption spectroscopy (TDS) was about $4x10^{-4}$ H/Ni (~7.5 wppm). This result is in agreement with previous experimental data available in the literature (Fukai, 2005; Lee and McLellan, 1984; Oudriss et al., 2012). The second method (the incorporation of hydrogen by the chemical way) consisted to immerse the specimens in an ammonium thiocyanate solution (NH_4SCN) with a concentration of 250g.L^{-1} for 24h at 323K. This inorganic compound is often used with a lower concentration as a poison to incorporate hydrogen in metal by the electrochemical way (Akiyama and Li, 2016). The temperature of the double-walled cell has been also kept constant during hydrogen charging and the concentration of hydrogen measured with TDS is about $8x10^{-4}$ H/Ni (~13 wppm).

Then, we have performed series of uniaxial cyclic tests on two pre-charged hydrogen concentration, the first one electrochemically charged (with $C_H = 4.10^{-4}$ H/Ni) and the second one chemically charged ($C_H = 8.10^{-4}$ H/Ni) besides the cyclic tests performed on pure nickel. The mechanical tests have been carried out on <001> oriented nickel single crystal specimens (20 mm x 4 mm x 1 mm and a gauge length of 10 mm) with a micro-tensile testing machine (Kammrath & Weiss, 5kN) at room temperature. The strain was controlled during the cyclic tests with an extensometer and strain rate has been kept constant at 2.10^{-5} s^{-1} in addition to the applied strain amplitude for all mechanical tests. These conditions induced an increase of the applied stress (measured with a 5kN tension/compression module) with the number of cycles until a stabilisation. This stabilisation suggests a homogenisation of the dislocation structures for a given plastic strain amplitude (Gentet, 2009; P. Li et al., 2011) and the mechanical tests have been therefore stopped.

2.2 Microstructural characterisation using transmission electron microscopy

We investigated the microstructure developed by the cyclic tests at several plastic strain amplitudes of pure nickel and electrochemically pre-charged nickel using TEM. The induced dislocation arrangement has been investigated using a JEOL JEM 2011 electron microscope operating at 200kV. Foils for TEM have been thinned in a double twin-jet electro-polisher using electrolytes at the conditions described previously (Feaugas, 1999; Miyata, 2003). Different plastic shear strain amplitudes have been observed in the present study, which is attributed to different cyclic hardening stages (II_0, III_0, III) with different dislocation features. The characterisation of the

developed dislocations structures with and without hydrogen has been determined statistically. This approach has been used in previous studies to describe the dislocation arrangement of polycrystalline nickel (Feaugas and Haddou, 2007; Hughes and Hansen, 2000) and nickel single crystal (Girardin et al., 2015; Oudriss and Feaugas, 2016). The dislocation densities ρ have been determined using standard intersection method (Amelinckx, S., 1971; Oudriss, 2012; Underwood, 1973) from TEM images collected by Digital Micrograph^{TM} software.

2.3 Nano-indentation details and contact mechanism

Nano-indentation (NI) tests have been performed on cyclically pre-strained nickel single crystal and nickel-hydrogen systems, which have been aged several months. All surfaces of each sample have been electropolished at room temperature during 20s with a potential of 30V in a 1M methanolic H_2SO_4 solution to remove the strained surface layer (Barnoush and Vehoff, 2010; Stenerud et al., 2017). The sample surfaces have been checked by scanning probe microscopy (SPM) to ensure the surface roughness was small enough to conduct the NI tests and the surface condition has been identified for all specimens (Barnoush and Vehoff, 2008). Then, the indents have been performed in a Hysitron Triboindenter with 90° cube-corner shaped tip. This tip was chosen because it has a smaller ideal projected area compared to Berkovich and 90° conical-shaped tips (Barnoush and Vehoff, 2008; Fischer-Cripps, 2007). The applied load function of each indentation consisted of a loading rate of $200\mu N.s^{-1}$ up to the maximum load of 50μN. The maximal load has been kept constant during 3s in order to observe any creep effect during the loading (Barnoush, 2008), then it has been reduced to 10% of the maximum load for 1.25s for drift correction (Stenerud et al., 2017). The feedback during testing has been set to open-loop (no feedback). In this way, no feedback has been used to control the load or the displacement during the testing (Ebenstein and Wahl, 2006).

Some series of NI tests have been linked to electron channeling contrast imaging (ECCI) in order to study the indents hitting the different dislocation structures developed from cyclic loading. The indents have been investigated *via* ECCI in the environmental scanning electron microscope (ESEM, Quanta 650 FEG, Thermo Fisher Scientific Inc., USA) (Hajilou et al., 2017; Wan et al., 2018). A solid-state four-quadrant backscatter electron (BSE) detector has been used at an accelerating voltage of 30kV. The contrast was controlled to an optimum state by using optimum working distance and tilting the specimen to a two-beam diffraction condition. The BSE contrast normally consists of the information from the atomic number and local misorientation. Since the investigated specimen had a uniform phase constituent, no atomic number information was released. In addition, since the specimen was prepared by electropolishing to remove the deformation layer from grinding and mechanical polishing, only the contrast from the local plastic strain (introduced by defects, *i.e.*: dislocations in the present study) could be observed in the present results. Therefore, this set-up is suitable and has been adopted to check the indents on the cyclically deformed area (Wan et al., 2018; Wan and Barnoush, 2019).

The load-displacement (L-D) curves of NI tests are separated in 3 stages, which are the elastic loading, the discrete transition between elastic and plastic regions (pop-in) and the continued elastoplastic loading (Barnoush and Vehoff, 2010, 2008). The initial elastic response, before the pop-in event, is described by the contact mechanism theory with the Hertzian fit (Hertz, 1881).

$$P = \frac{4}{3} E_r \sqrt{R h^3} \tag{1}$$

with P and h the indentation load and depth, respectively. The reduced Young's modulus E_r has been determined accordingly to the Oliver and Pharr method (Oliver and Pharr, 1992; Renner et al., 2016; Vlassak and Nix, 1994). From equation (1), the indenter tip radius R has been calculated and

used to determine the maximum contact pressure p_0 with the following expression (Barnoush, 2008; Gao and Bei, 2016; T. L. Li et al., 2011):

$$p_0 = \left(\frac{6P_{pop-\text{in}}E_r^2}{\pi^3 R^2}\right)^{1/3} \quad (2)$$

with $P_{pop-\text{in}}$ the applied load when the pop-in occurred. The orientation effect of the crystallographic plan was pointed out in the literature experimentally and numerically in the case of FCC crystals (Liu et al., 2008; Renner et al., 2016). Therefore, Gao and co-workers introduced an indentation Schmid factor for circular contact $S_{(hkl)}$ in order to evaluate the maximum resolved shear stress acting on slip systems at the onset of plasticity (Gao and Bei, 2016; T. L. Li et al., 2011):

$$\tau_{max}^{RSS} = p_0 \times S_{(hkl)} \quad (3)$$

with (hkl) the crystallographic plane of the material. S_{001}= 0.243 in case of indentation of (001) crystallographic plane to activate a/2<011>{111} slip systems for nickel single crystal (T. L. Li et al., 2011).

3. Results

3.1 Cyclic response

The uniaxial cyclic tests have been performed on nickel single crystal with several hydrogen concentrations (0 H/Ni, 4x10^{-4} H/Ni, 8.10^{-4} H/Ni) until we observed a negligible variation of the stress with the number of cycle N (saturation state). **Figure 1** presents the amplitude of shear stress τ as a function of the ratio N/N$_T$ with N$_T$ (equal to at least 300 cycles when γ_P=7x10^{-4} and 150 when γ_P=25x10^{-4}) for nickel and nickel-hydrogen systems. When the variation of the stress is negligible (stationary state), hysteresis loops of samples with and without hydrogen is obtained and presented in **supplementary material 1**.

At low plastic strain amplitude (γ_P=7x10^{-4}), the amplitude of shear stress of the last cycle for Ni-H systems is lower than the stress of the last cycle for pure Ni. However, at larger plastic strain amplitude (γ_P=25x10^{-4}), a minor increase of this stress is observed when the solute is pre-charged into the host metal. Then, we have determined the saturated stress τ_{as} for a given plastic shear strain amplitude γ_P for Ni, Ni-H$_{0.0004}$ and Ni-H$_{0.0008}$. These values are all regrouped in **table 1**, which also specifies which samples have been analysed using TEM and NI after the cyclic deformations.

The cyclic stress-strain curves (CSSC) of nickel with and without hydrogen were obtained from the analysis of the hysteresis loops and they are presented in **figure 2**. In the case of pure nickel, the results are in good agreement with data from the literature (Bouteau, G., 2013; Buque, 2001). In addition, the cyclic hardening curve of nickel highlights the different hardening stages which are I, II$_0$, III$_0$ and III and corresponds to the predominance of a dislocation organisation (Li et al., 2009; P. Li et al., 2011).

When hydrogen has been introduced by chemical and electrochemical ways, a competition between softening and hardening is noted with the plastic strain amplitude. A decrease of the saturation stress is observed for stages II$_0$ and III$_0$ (γ_P < ~3.10^{-3}) and a minor increase of τ_{as} is obtained in stage III. Although a larger hydrogen concentration is noted when the solute is introduced chemically, the cyclic stress-strain curves of both nickel-hydrogen systems are similar.

Thus the hydrogen concentration seems to have a minor effect on τ_{as}. In addition, the introduction of hydrogen in nickel single crystal shifts the transition between the stages II_0 and III_0 at larger plastic strain amplitudes. This result is a macroscopic evidence of the effect of the solute on the decrease of the cross-slip probability, already observed on single slip oriented nickel single crystal in the literature (Castelluccio et al., 2018; Delafosse, 2012; Magnin et al., 2001).

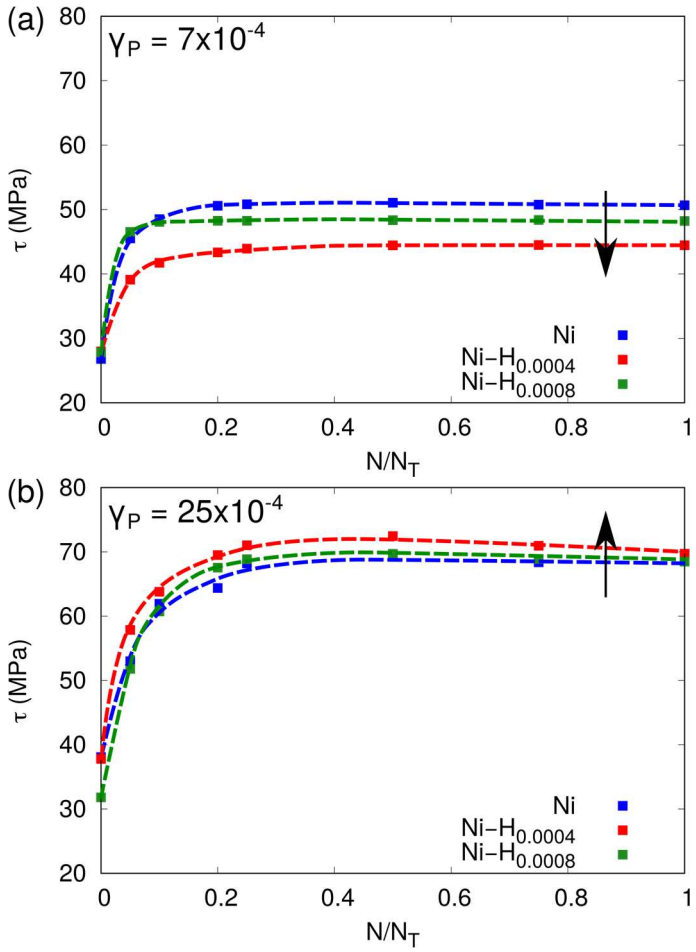

Figure 1: Shear stress as function of the ratio N/N_T when the plastic strain amplitude is equal to 7x10^{-4} (a) and 25x10^{-4} (b). The shear stress τ and shear strain γ have been deduced to longitudinal cyclic stress-strain curve (σ, ε) using geometric considerations (Schmid and Boas, 1950): $\tau = 0.4 \times \sigma$ and $\gamma = \varepsilon/0.4$.

Table 1: Fatigue test data for nickel-hydrogen systems with several hydrogen concentrations (0 H/Ni, 4x10^{-4} H/Ni and 8x10^{-4} H/Ni) with a loading axis parallel to the <001> direction, with N_T the total number of cycles.

Material	Specimen Number	N_T	γ_P (1x10^{-4})	τ_{as} (MPa)	Technique used after the cyclic test
Ni	A1	450	0.3	25.6	
	A2	300	1.5	34.8	TEM
	A3	300	1.7	38.3	
	A4	300	2.5	42.8	NI
	A5	250	7.1	55.6	

	A6	200	12.7	64.2	TEM
	A7	150	14.0	58.8	NI
	A8	150	25	60.8	NI
	A9	100	49.3	78.1	TEM
	A10	100	50.9	72.1	NI
Ni-$H_{0.0004}$ (hydrogen pre-charged electrochemically)	B1	500	2	31.5	TEM
	B2	500	2.2	36.3	
	B3	200	4.7	46	
	B4	200	6.2	45.2	
	B5	200	7.5	52.2	NI
	B6	150	8.1	52.1	
	B7	150	8.9	55.3	
	B8	150	9.9	56.8	TEM
	B9	150	20.5	61.1	NI
	B10	150	25	62.8	
	B11	150	32.5	69.6	NI
	B12	150	47.6	64.9	
	B13	100	50.3	70.5	TEM
Ni-$H_{0.0008}$ (hydrogen pre-charged chemically)	C1	500	2.5	38.5	
	C2	300	6.7	51.8	
	C3	150	25	61.9	
	C4	150	32	68.9	

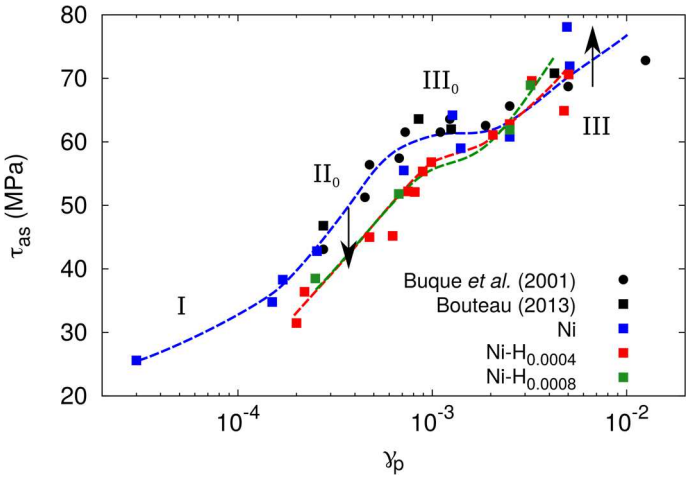

Figure 2: Cyclic stress-strain curves of pure Ni and Ni-H systems at different plastic shear strain amplitude. The different hardening stages I, II_0, III_0 and III are indicated. A comparison with the literature is also provided for <001> oriented Ni (Bouteau, G., 2013; Buque, 2001).

3.2 Internal stresses

The saturation stress has been decomposed in terms of effective and back stresses (τ_{eff} and τ_X, respectively) and evaluated from the hysteresis loops of each mechanical tests according to the method proposed in the work of Dickson *et al.* (Dickson et al., 1984, 1983) and thoroughly discussed in the work of Feaugas *et al.* (Feaugas, 2003, 1999; Feaugas and Haddou, 2007). The effective stress represents the short-range interaction of dislocations, its mobility is affected by the elastic field of the cross object only when it is close to this one. In contrast, the back stress represents the long-range interactions of the defect, which is modified by the elastic field of the cross object well before being near this one (Feaugas, 2003; Kassner et al., 2013; Mughrabi et al., 1986).

The determination of the effective and back stresses has been performed on the hysteresis loops of nickel single crystals with and without hydrogen (an example is given in **supplementary material 1**) and the results are represented in **figure 3** as a function of the plastic strain amplitudes. We note the solute reduces the stress τ_{eff} for all plastic strain amplitudes and this reduction is larger with the hydrogen concentration (**figure 3(a)**). Consequently, hydrogen addition reduces the short range elastic interactions between dislocations. Thus, this result suggests that hydrogen increases the mobility of dislocation locally for every plastic deformation and supports the HELP mechanism. The latter characterised hydrogen embrittlement with an increase of emission and mobility of dislocations in the presence of the solute according to the shielding model. The behaviour of the back stress seems more complex because it depends on the plastic strain amplitude and the hydrogen concentration (**figure 3(b)**). We note a minor softening of the back stress at the cyclic hardening stage II_0 (γ_P < ~1.10^{-3}) and a hardening of the back stress beyond this limit when hydrogen has been introduced electrochemically. This change of behaviour should be associated with other microstructural characterisations in order to understand the processes acting on τ_X. Finally, when hydrogen has been introduced chemically at a larger concentration, a significant hardening of the back stress is noted for all plastic strain amplitudes.

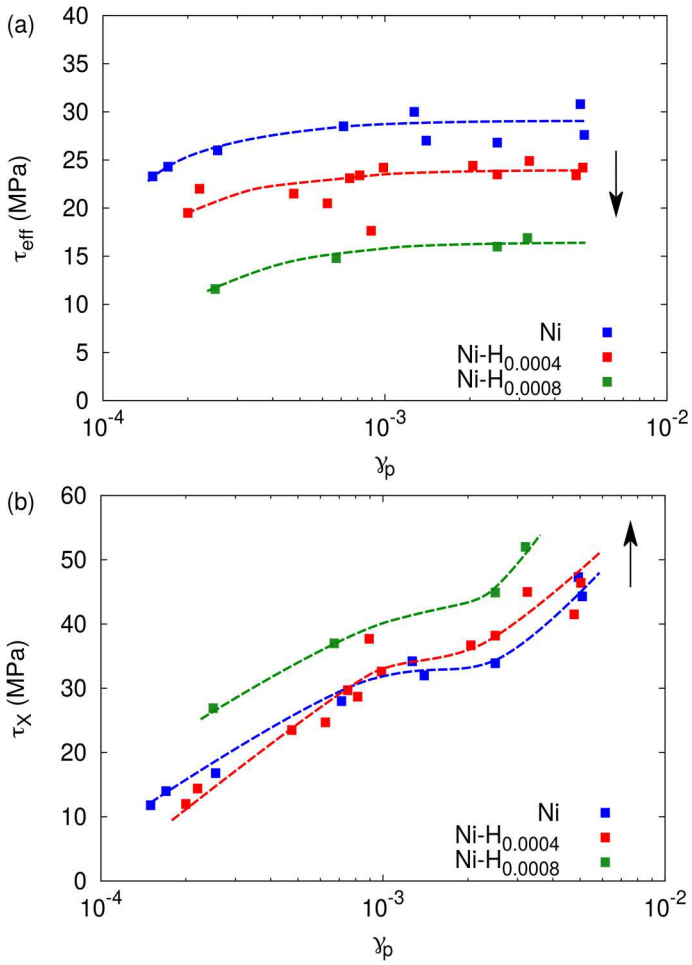

Figure 3: Influence of hydrogen on the effective stress τ_{eff} (a) and back stress τ_X (b) of nickel single crystal. The black arrows highlight the effect of the solute on the internal stresses.

3.3 Dislocations organisation

The microstructures associated with the cyclic hardening stages II_0, III_0 and III of nickel single crystal and nickel-hydrogen systems pre-charged electrochemically have been observed using TEM and their microstructures are presented in **figure 4**. The dislocation organisation developed for all hardening stages is in agreement with the literature (Argon, 1996; Laird, 1996; P. Li et al., 2011). It is separated into two phases (wall and channel phases), as previously detailed (Mughrabi, 1988, 1987, 1983). The nickel-hydrogen systems have been pre-charged electrochemically during 72h, inducing a hydrogen concentration of $4x10^{-4}$ H/Ni before the cyclic tests. Then, the samples have been aged several weeks at room temperature before the TEM observations.

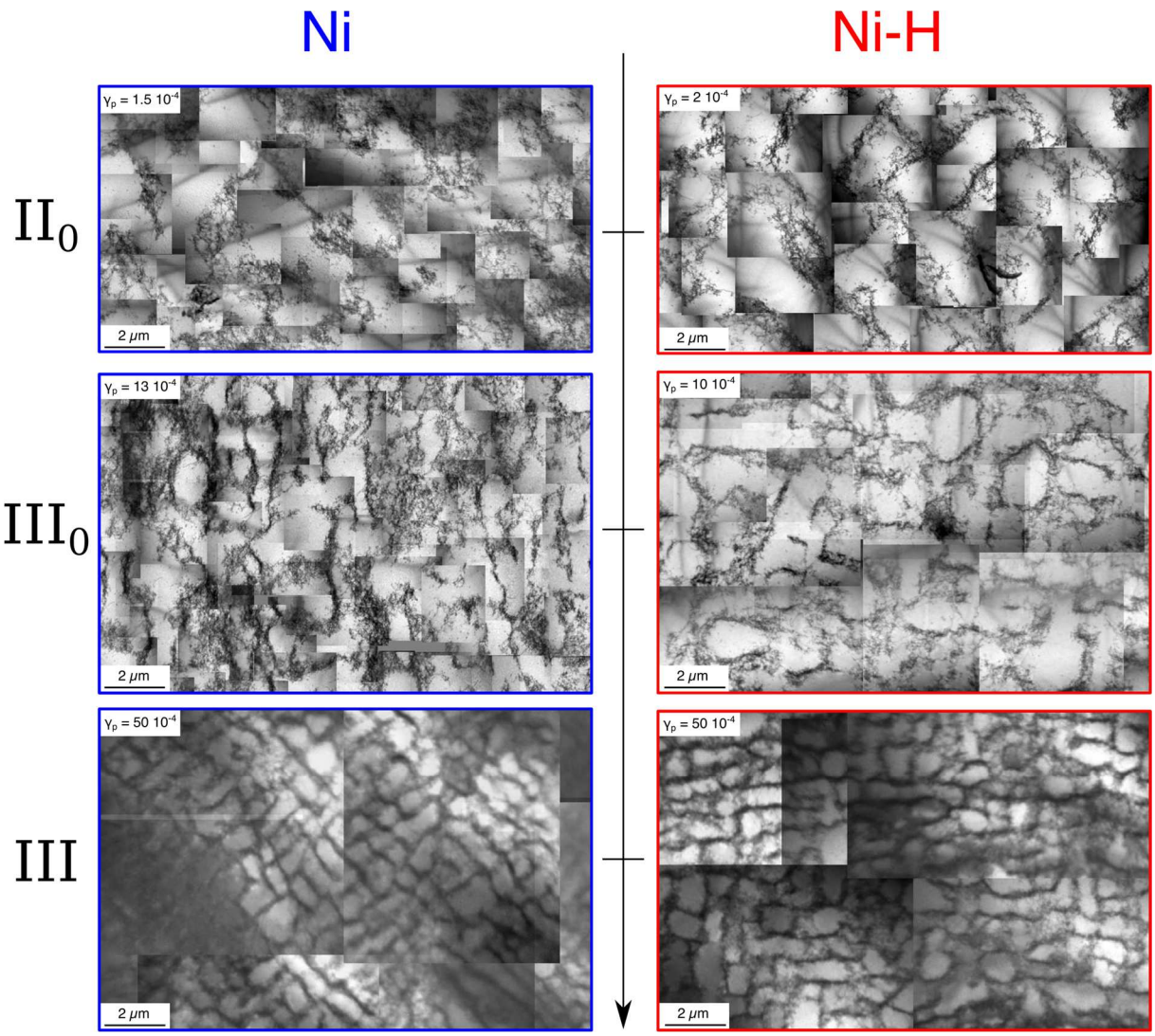

Figure 4: Microstructure induced by cyclically strained nickel (left) and nickel-hydrogen systems (right) at stages II_0 (top), III_0 (middle) and III (bottom).

The first comparison of the TEM images reveals no significant qualitative difference between the dislocation organisation of nickel and nickel-hydrogen systems. This observation suggests that the solute has a minor impact on the microstructures induced by fatigue when its initial hydrogen concentration is $4x10^{-4}$ H/Ni. We have effectuated a throughout statistical analysis of the distribution of each microstructure and evaluated their dislocations density for all TEM images in order to discuss the quantitative impact of hydrogen on the dislocations organisation. During this study, we have evaluated the size distribution of each phase (wall and channel) for both systems at each cyclic hardening stage (more than 150 measurements have been performed for one distribution). **Supplementary material 2** presents the size distribution of walls e and channels λ of nickel and nickel hydrogen systems for all stages. The average sizes of the wall $<e>$ and channel $<\lambda>$ have been determined from these distributions and we have calculated the fraction of walls with the following equation (Oudriss and Feaugas, 2016):

$$f_w = \frac{<e>}{<e> + <\lambda>} \qquad (4)$$

The different fractions of wall structures of cyclically pre-strained Ni and Ni-H systems are presented in **table 2**. For all the hardening stages, the fraction of wall phase decreases with the

incorporation of hydrogen. This behaviour is mostly due to a decrease of the inter-wall spacing (see **supplementary material 2** for more information).

Table 2: Fraction of walls f_w in nickel with and without hydrogen for the different cyclic hardening stages.

	Stage II_0	Stage III_0	Stage III
Ni	34.2 %	27.9 %	28.7 %
Ni-H	16.7 %	25.5 %	23.9 %

Then, the dislocations densities in the wall (ρ_w) and channel (ρ_c) phases have been determined and the results are represented in **figure 5**. At least, 15 grids with a total length L_T of 100µm (for some measurements total length of the grid was equal to 300µm) have been superimposed on each phase of a strained sample in order to obtain a representative result of the dislocations density.

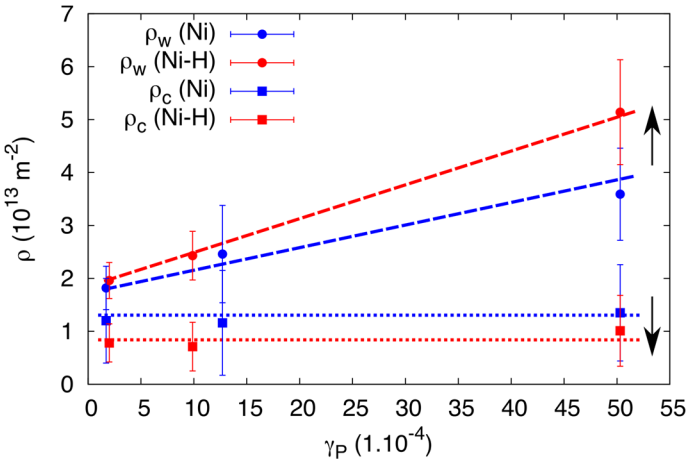

Figure 5: Measured dislocation densities in wall (ρ_w) and channel (ρ_c) structures for the stages II_0, III_0 and III of pure Ni (blue) and Ni-H systems (red).

The standard deviation of dislocation density in channel phases is relatively large (> 60 % for some cases) for each ρ_c measured because the defects are less visible in this phase. This observation has already been pointed out in a previous study (Oudriss and Feaugas, 2016). However, the consequence of the defect is still noted for all phases in the different hardening stages. Indeed, we observe a decrease of the dislocations density in channels ρ_c and an increase of ρ_w when hydrogen has been pre-charged in nickel single crystal for all plastic strain amplitudes.

These statistical studies present a significant impact of hydrogen on the dimensional characteristics of the induced heterogeneities (f_w), but also on the dislocations densities (ρ_w and ρ_c). Nevertheless, it is decisive to evaluate the impact of the solute on the local mechanical characteristics of each microstructure. Therefore, NI tests have been performed on pre-strained nickel single crystals with and without hydrogen at several plastic strain amplitudes.

3.4 Nanoindentation with ECCI

First, NI tests with ECCI have been performed on the pre-strained sample in order to individualise the mechanical behaviour of indents when they hit the different induced dislocation phases. **Figure 6(a)** presents the indents conducted of sample B5 (table 1), which is a cyclically pre-strained nickel-hydrogen system with a plastic strain amplitude of 7.5 x 10^{-4}. This sample is at the transition between stages II_0 and III_0, where dipolar walls are visible. For this series of 25 indents, 4 presented non-usable L-D curves, 5 indents hit a wall phase (which are represented with blue

numbers), 11 touched a channel phase (which are represented with red numbers) and the last 5 indents hit a channel too close to a wall phase (they are represented with green numbers) and were therefore not taken into account. The corresponding L-D curves of the indents hitting the wall and channel phases are represented in **figure 6(b)**. A tip radius R of 181 nm has been evaluated from the Hertzian fit applied to the elastic part of these curves (until $P_{pop-\text{in}}$ for each curve). R has been kept constant in order to determine the reduced Young's modulus E_r.

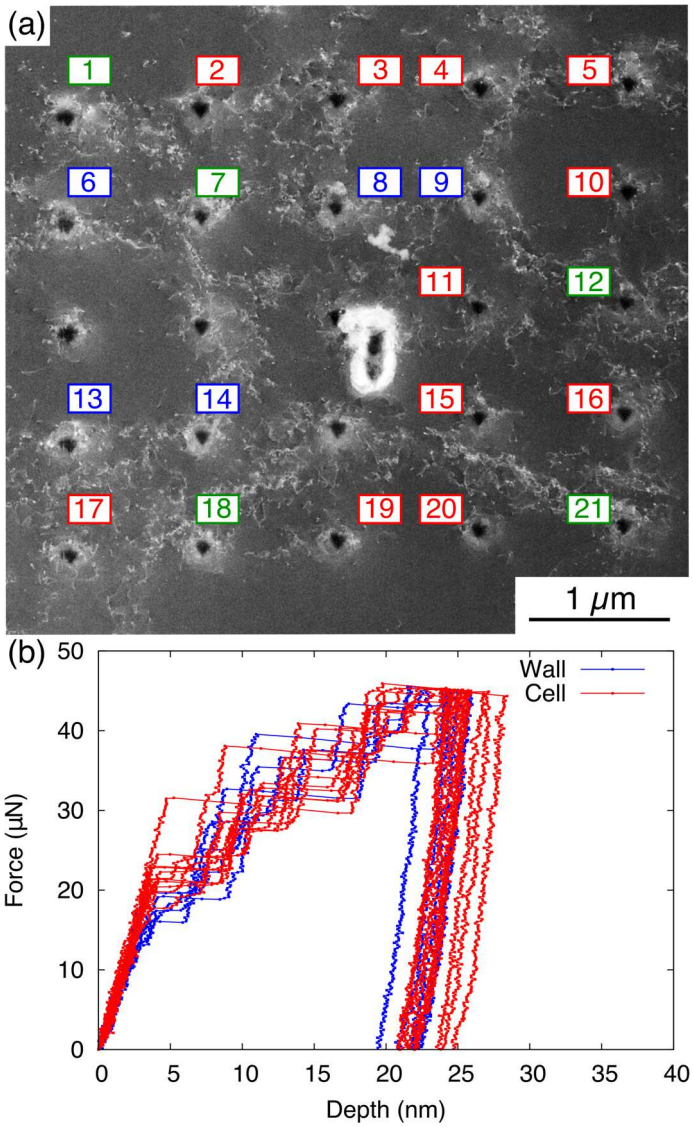

Figure 6: ECCI of indents made on cyclically pre-strained Ni-H systems (γ_P=7.5 x 10^{-4}) (a). Corresponding load-displacement curves of indents that are hitting wall or channel phases (b).

Table 3 presents the results when the indenter hits wall and channel phases. We note a minor variation of the reduced Young's modulus (<10 %) between both microstructures. It can be explained because the reduced Young's modulus has been evaluated from the unloading part of the L-D curves where the plastic zone of the indent is beyond the dimensional limits of the different phases. However, a difference of average value is obtained for the pop-in load $P_{pop-\text{in}}$, which is transmitted on the maximum resolved shear stress τ_{max}^{RSS}. We note a deviation of ~16% between the average values of τ_{max}^{RSS} of the indents in a wall or a channel phase. Moreover, one can note that larger critical stress is obtained when the indenter hits a channel phase than the wall phase, such counter-intuitive result is discussed in the next section. Therefore, a statistical study has been performed to identify the average behaviour of indenter touching the different microstructure at different hardening stages of nickel single crystals with and without hydrogen.

Table 3: Pop-in load, reduced Young's modulus and maximum resolved shear stress of the different indents hitting wall and channel phases of cyclically pre-strained Ni-H systems.

	Indent Number	P_{pop-in} (µN)	E_r (GPa)	τ_{max}^{RSS} (GPa)
Indenter hitting wall structures	6	17.40	172	3.52
	8	11.31	208	3.47
	9	18.89	163	3.50
	13	16.03	179	3.53
	14	19.51	155	3.41
	<•>	**16.63**	**175**	**3.49**
Indenter hitting channel structures	2	22.81	188	4.10
	3	17.79	215	4.12
	4	31.49	188	4.56
	5	24.45	178	4.04
	10	19.47	183	3.81
	11	20.81	178	3.84
	15	22.27	187	4.04
	16	20.49	211	4.26
	17	21.32	179	3.87
	19	22.80	207	4.36
	20	19.65	200	4.06
	<•>	**21.63**	**191**	**4.04**

3.5 Statistical study on the maximum resolved shear stress of wall and channel structures

We previously observed different average maximum stresses $<\tau_{max}^{RSS}>$ depending on where the indenter hits the dislocation organisation induced by fatigue. Therefore, we choose to perform a statistical study of $<\tau_{max}^{RSS}>$ on cyclically pre-strained Ni and Ni-H systems at different plastic strain amplitude (specimens presented in **table 1**) in order to analyse the evolution of the internal stress induced by the different phases with and without hydrogen. Moreover, we have performed a statistical study on nickel single crystal without any deformation, which is used as a reference state in this study. **Figure 7(a)** presents the $<\tau_{max}^{RSS}>$ distribution of more than 100 indents, which has been hitting the reference state sample. The black curve with red dots represents a fitted Gauss function f_G:

$$f_G = A \times exp\frac{-(\tau_{max}^{RSS} - <\tau_{max}^{RSS}>)^2}{2\sigma^2} \quad (5)$$

with A the maximum amplitude of the curve, $<\tau_{max}^{RSS}>$ and σ^2 the average maximum resolved shear stress and the variance of the distribution, respectively. In case of nickel without any deformation, we obtain $<\tau_{max}^{RSS}>$ = 3.9 GPa with equation (5) and **figure 7(a)**. This value corresponds to the

critical stress required to nucleate dislocations in a homogenous medium, without initial strain. Then, at least 60 indents have been analysed on the pre-strained samples in order to determine the $<\tau_{max}^{RSS}>_i$ distributions of cyclically pre-strained Ni and Ni-H samples presented in **supplementary material 3**. When the sample is cyclically pre-strained at stages III_0 and III, the τ_{max}^{RSS} distribution is systematically deconvoluted into two Gauss functions (an example is given in **figure 7(b)**), related to the dislocation structures of each phase.

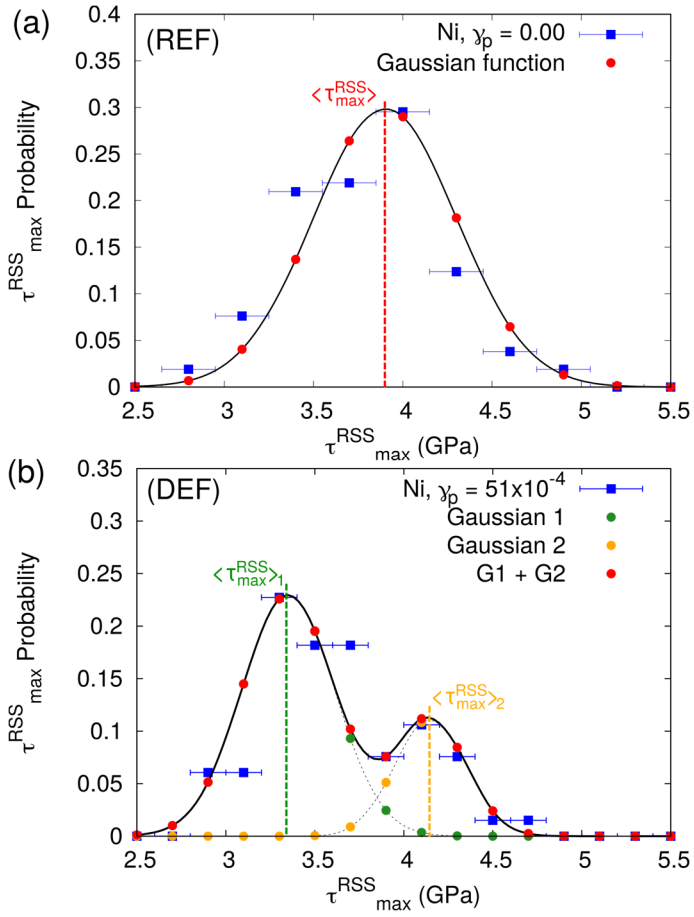

Figure 7: Maximum resolved shear stress distribution of a {001} oriented pure nickel without hydrogen (reference state). Corresponding Gaussian function which fit the measured data (a). Typical τ_w distribution of cyclically pre-strained sample at stages III_0 or III. Two Gauss functions are used to fit the measured data (b).

Then, we evaluated the average maximum stresses $<\tau_{max}^{RSS}>_1$ and $<\tau_{max}^{RSS}>_2$ from those Gauss functions for each distribution and correspond the average maximum stress when the indenter hits the different phases ($<\tau_{max}^{RSS}>_1 = <\tau_{max}^{RSS}>_w$ and $<\tau_{max}^{RSS}>_2 = <\tau_{max}^{RSS}>_c$) . The measured average maximum stress and standard deviation of all distributions are reported in **table 4**.

Table 4: Measured average stresses $<\tau_{max}^{RSS}>_i$ and standard deviations σ_i of the different strained structures in nickel and nickel-hydrogen systems.

		$<\tau_{max}^{RSS}>_w$ (GPa)	σ_w (GPa)	$<\tau_{max}^{RSS}>_c$ (GPa)	σ_c (GPa)
III_0	Ni	3.57	0.07	4.2	0.04
	Ni-H	3.28	0.03	3.8	0.03

III	Ni	3.35	0.04	4.15	0.07
	Ni-H	3.3	0.07	4.1	0.05

NI tests have been conducted on cyclically pre-strained pure nickel and nickel-hydrogen systems at several stages. We note a stress distribution similar to a Gaussian function for nickel without any deformation, pre-strained nickel and nickel-hydrogen systems in stage II_0. When the mechanical tests have been performed on pre-strained samples in stages III_0 and III, a deconvolution of the distribution is obtained with the mean values of τ_{max}^{RSS} represented in **table 4**. According to the NI tests conducted with the ECCI, the deconvolution of the distribution is induced by the different phases (wall and channel). Therefore, it is possible to determine internal stress needed to emit dislocations in each phase and it is presented in the next section.

4. Discussion

In the present work, we have performed uniaxial cyclic tests on <001> oriented nickel single crystals with and without hydrogen. We have noted a competition between softening and hardening of the metal in the presence of the solute depending on the plastic strain amplitude at the macroscale. Then, we have performed a statistical study of the dislocation organisation observed using TEM and internal stresses using NI at the microscale. The first part of this discussion is dedicated to these results from both length scales in order to evaluate the stress induced by each phase in all hardening stages for pure nickel and nickel-hydrogen systems. In the second part of this section, we discuss the results obtained from TEM analysis with the maximum resolved shear stress determined using NI.

4.1 Effect of hydrogen of the stress induced by the different phases

The uniaxial cyclic tests performed on multi-slips oriented nickel single crystal with different hydrogen concentrations presented a softening of the metal for the hardening stages II_0 and III_0 with a delay of deformation III_0 when the solute is incorporated. These observations are similar to the ones noted for cyclically strained nickel single crystal oriented for single slip in previous studies and have been affiliated to a delay of cross-slip events in the presence of hydrogen (Delafosse, 2012; Magnin et al., 2001). However, at larger plastic strain amplitude (at stage III), we have observed a minor hardening of the metal with hydrogen. In order to explain such behaviour, we have calculated the internal stresses representing the short and long-range interactions of dislocations from the different hysteresis loops. We noted the effective stress (stress increased by dislocations in channel phase) decreases with the hydrogen concentration, in another term, a decrease of the elastic interactions between dislocations which significates a possible increase of the dislocation mobility locally and supports the proposed HELP model. The consequence of hydrogen on the back stress is more complicated to explain, therefore a TEM characterisation of the dislocation organisation of pure nickel and nickel-hydrogen systems electrochemically pre-charged has been performed. From the statistical study performed on the TEM micrographs of cyclically pre-strained Ni and Ni-H systems, we observed that hydrogen reduces the fraction of wall structures but increases the dislocations density in this phase. Furthermore, the solute decreases the dislocations density in channel structures for a given plastic strain amplitude.

Moreover, from the internal stresses evaluated with the hysteresis loops at macroscale and the microstructural characterisation of the previous section, it is possible to determine the stress induced by each phase τ_w and τ_c. The microstructures of cyclically pre-strained nickel single crystals with and without hydrogen are similar to dislocation structures observed in the literature in the case of FCC crystals. Therefore the plastic flow is easier in the channel than in the wall phase (Feaugas, 2003; Mughrabi, 1988, 1983). Hence, we can suppose:

$$\tau_c = \tau_{eff} \tag{6}$$

with τ_c the stress induced by the channel phase and τ_{eff} the effective stress determined previously. Besides, we have noted the dislocation organisation induced by fatigue is composed of 2 phases for all plastic strain amplitudes. Therefore, we suppose the mechanical behaviour of the different phases is also similar to a composite (Feaugas, 2003; Mughrabi, 1988, 1983), hence:

$$\tau_{as} = f_w \times \tau_w + (1 - f_w) \times \tau_c \rightarrow \tau_w = \frac{\tau_{as} - (1 - f_w) \times \tau_c}{f_w} \tag{7}$$

with τ_w the stress induced by wall structure. **Figure 8(a)** presents the different stresses induced by each phase as a function of the plastic strain amplitude for nickel and nickel-hydrogen systems. The evolution of the stress-induced by both phase is similar to the evolution of the dislocation densities with the incorporation of the solute. We note an increase of the stress induced by wall structures and a decrease of the stress-induced by the channel structures in the presence of hydrogen.

Since, hydrogen has the same effect on dislocations densities and stress induced by each phase for all plastic strain amplitudes, the α-factor defined as the ratio of both values can be evaluated with the following equation (Mughrabi, 2016; Nabarro et al., 1964; Taylor, 1934).

$$\alpha_i = \frac{\tau_i}{\mu b \sqrt{\rho_i}} \tag{8}$$

with μ and b the isotropic shear modulus (equal to 96 GPa from the elastic constants determined by DFT calculations in previous work (Hachet et al., 2018)) and the Burgers vector of a dislocation (equal to 0.25 nm). **Figure 8(b)** presents the evolution of this factor, which represents a global hardening of the metal due to dislocation interactions. Moreover, we assumed the shear modulus did not vary for nickel-hydrogen systems since we quantified a minor effect of hydrogen on the elastic properties of nickel single crystal in previous work (Hachet et al., 2018, 2019). In this study, the calculated factor remained between $0.2 \leq \alpha_i \leq 0.45$ for both phases at all plastic strain amplitudes for nickel with and without hydrogen. This result is in agreement with the literature, notably the synthesis work of Mughrabi (Mughrabi, 2016). Moreover, even if α_i seems to decrease with the plastic deformation, an increase of the factor is noted in these works between the stages II_0 and III_0, this is mostly due to an increase of τ_i larger than $\sqrt{\rho_i}$. Finally, we have observed a minor difference between α_i(Ni) and α_i(Ni-H) for all plastic strain amplitudes, suggesting that hydrogen has a negligible effect on the hardening coefficient of dislocations coefficient induced by fatigue.

From this multi-scale analysis, we observed that hydrogen increases the dislocations density and the stress induces by wall structures, which means that hydrogen hardens this dislocation structure. However, the solute reduces the dislocations density and the stress induces by channel structures and softens this phase. In order to comfort those results, we compare them with the nanoindentation results, where we have distinguished different mechanical behaviour depending on where the indenter has hit the microstructure. This subject is discussed in the next section.

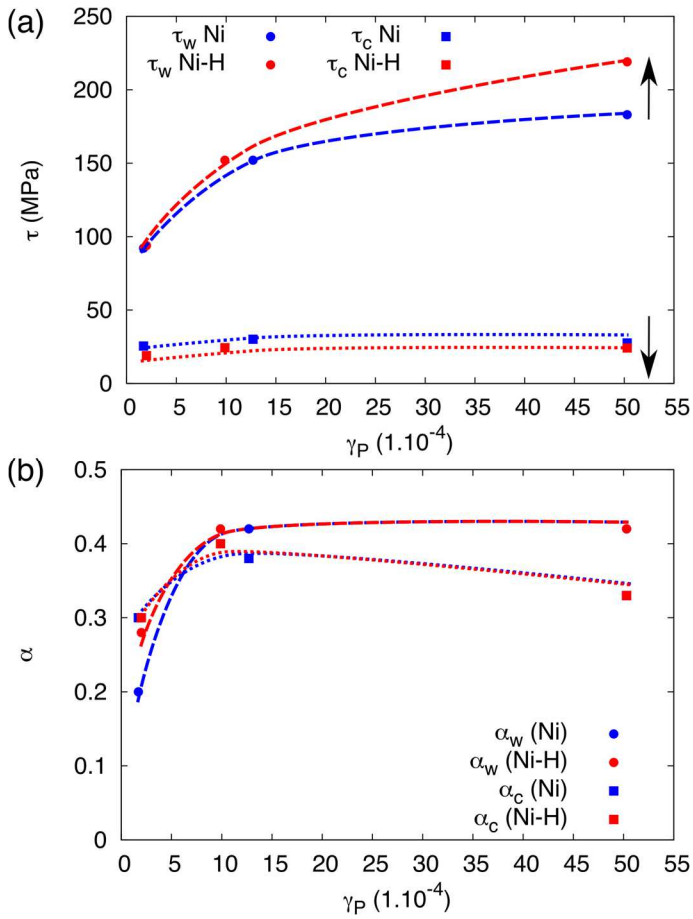

Figure 8: Stress (a) and geometrical α-factor (b) induced by wall and channel phases for the hardening stages II_0, III_0 and III for pure nickel (blue) and Ni-H systems (red).

4.2 Deconvolution of the pop-in distribution due to the different phases

The NI investigation focused on the discrete onset of the plasticity of L-D curves when the indenter hits different microstructures. We noted an increase of this critical stress when the indenter touched a channel phase and a decrease when it touched a wall phase by performing NI tests with ECCI. This difference of behaviour can be affiliated with different pop-in mechanisms presented in the literature (Bei et al., 2016; Gao and Bei, 2016). In their work, they observed strain-softening and strain-hardening mechanisms in the single crystal by changing the size of the indenter tip (which change the stressed volumes). When dislocations were present within the stressed volume of the indenter, they acted as nucleation sources for pop-in events and reduced the measured strength from the theoretical value for pop-in events. This configuration is similar to the situation where the indenter touched the wall phase in our study. The large dislocations density served as nucleation sources, which has reduced the maximum stress τ_{max}^{RSS}. Hence, even though the wall phase is a dislocation rich area, a lower maximum stress is obtained. Moreover, in the work of Bei *et al.*, a strain-hardening mechanism has been also observed due to an increase of the dislocations density and correspondingly the yield stress increased, at the bulk limit (Bei et al., 2016; Gao and Bei, 2016). This situation is close to the observed configuration in this work, when the indenter touched channel structures. The stress fields induced by dislocations led to an increase of the critical stress τ_{max}^{RSS} but the dislocations density is too small for them to act as nucleation sources. These mechanisms are valid for NI tests, where long-range stresses are measured in the dislocation phase at the early stage of plasticity (*i.e.*: first pop-in indent) on a surface perpendicularly to the axial stress. Hence, when the indent hit the channel phase, the indenter compressed a structure compressed by the long-range interactions of wall phase. Such mechanical tests induced an increase of the critical stress, which has been observed for all NI tests. However, the noted effect stands for

long-range internal stress only. During the fatigue tests, the plastic flow is still easier in channel than in wall phases.

A statistical study has been performed on cyclically pre-strained nickel and nickel-hydrogen systems with different plastic strain amplitude. The distribution of the critical stress τ_{max}^{RSS} of strain-free and hydrogen-free nickel had a Gaussian shape and the average $<\tau_{max}^{RSS}>$ has been evaluated at 3.9 GPa. It corresponds to the stress needed to nucleate dislocations in a homogeneous environment in pure nickel. When the metal is pre-strained at stages III_0 and III, a deconvolution of the distribution into two Gaussian functions has been noted for pure nickel and nickel-hydrogen systems. Each Gaussian function corresponds to the indenter hitting one phase induced by cyclic tests and has been confirmed with the NI series linked with ECCI. From the average maximum stresses $<\tau_{max}^{RSS}>_i, i \in \{c, w\}$ of the different distributions, the long-range internal stress the different microstructure $\tau_{Xi}, i \in \{c, w\}$ can be evaluated according to **figure 9(a)** and obtained with the following equation:

$$<\tau_{max}^{RSS}>_i = \tau_{max}^{RSS} \pm \tau_{Xi}, i \in \{c, w\} \quad (9)$$

with τ_{max}^{RSS} equal to 3.9 GPa. The long-range internal stresses τ_{Xi} is linked to the induced heterogeneities from the dislocation structures developed with fatigue. **Figure 9(b)** presents the corresponding long-range internal stress of the different structure from the composite model, which can be determined from the TEM results with the following equations (Feaugas and Gaudin, 2001; Mughrabi, 1983; Oudriss, 2012):

$$\tau_{Xc} = \mu b f_w \left(\alpha_w \sqrt{\rho_w} - \alpha_c \sqrt{\rho_c}\right)$$
$$\tau_{Xw} = \tau_{as} - \tau_w \quad (10)$$

Table 5 presents τ_{Xi} evaluated from the τ_{max}^{RSS} distributions available in **supplementary material 3** and τ_{Xi} calculated from equation (10).

Table 5: $\tau_{Xc}$and τ_{Xw} determined using NI and TEM for pre-strained nickel and nickel-hydrogen systems at stages III_0 and III.

		NI		TEM	
		τ_{Xc} (MPa)	τ_{Xw} (MPa)	τ_{Xc} (MPa)	τ_{Xw} (MPa)
III_0	Ni	300	350	34	88
	Ni-H	100	400	32	95
III	Ni	300	450	46	110
	Ni-H	200	550	45	148

We note that similar results are obtained on the impact of hydrogen on the long-range internal stresses of wall and channel phases with both approaches. When the solute is incorporated, τ_{Xc} is reduced and τ_{Xw} is increased for both stages III_0 and III. Therefore, hydrogen softens channel phase, while it hardens the wall phase. Finally, **figure 9(c)** presents a comparison of the long-range stresses induced by each phase in nickel and nickel-hydrogen systems measured using TEM and NI. We noted also a good correlation between the long-range stresses determined with both techniques, which can confirm the results with both approaches. However, a correction factor equal to 4.13 is still needed. This difference should depend on a transition scale factor, which has not been taken

into account with τ_{Xi} determination from the τ_{max}^{RSS} distributions. During TEM, the measurement of the back stress is performed on the dislocation structures induced by fatigue in its loading direction. As for NI, the indents are performed on a plane, which is in a different direction (the normal is perpendicular to the loading direction). The induced dislocation structures are anisotropic and consequently the long-range internal stresses should be anisotropic and induced probably this factor. A finite element analysis should be performed in order to calibrate this factor. This work is in progress.

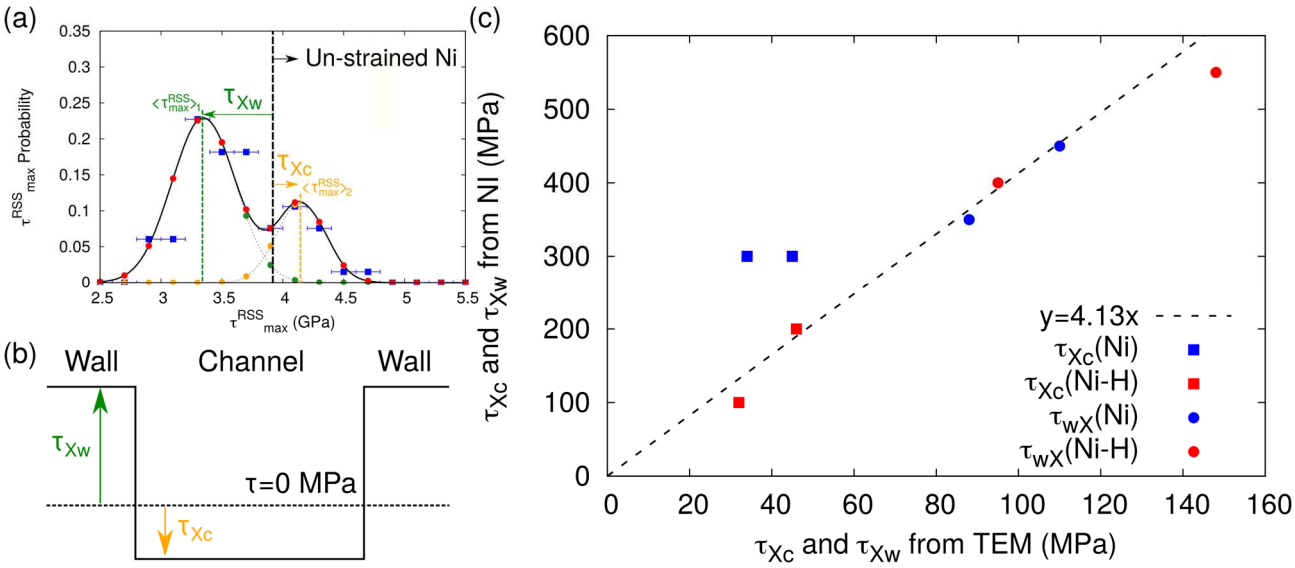

Figure 9: Long-range stresses evaluated from maximum resolved shear stress distribution (a). Equivalent long-range induced by wall and channel phases (Feaugas and Gaudin, 2001; Mughrabi, 1983) (b). Comparison between long-range stresses determined using TEM and NI techniques (c).

5. Conclusion

To summarise this study, we have performed cyclic tests <001> oriented nickel and nickel-hydrogen systems with two hydrogen concentration. We observed that hydrogen softens the metal at stages II_0 and III_0 and induces a minor hardening at stage III. The hardening and softening effects have been discussed in terms of effective and back stresses partitioning. The softening effect has been attributed to a reduction of the short-range interactions (decrease of effective stress τ_{eff}) leading to an elastic shielding, which is in relation with the HELP embrittlement model. A more complex behaviour has been observed for the back stress τ_X, which needs further investigations at lower length scale.

From the TEM characterisations, fatigue tests induce a dislocation organisation similar for nickel and nickel-hydrogen systems, which correspond to a composite structure composed of wall and channel phases. In the presence of the solute, we observed the fraction of the wall phase is always reduced for all plastic strain amplitudes. Besides, we also noted hydrogen increases the dislocations density and the stress induce by wall phase but decreases the dislocations density and the stress induces by channel phases for all plastic strain amplitudes. Hence, hydrogen hardens the wall phase while softening the channel phase.

We have also performed NI linked with ECCI on cyclically pre-strained nickel and nickel-hydrogen systems in this study. We have highlighted different pop-in mechanisms depending on the dislocation structures of the material and evaluated their long-range internal stress for different

plastic strain amplitudes. Similar behaviours have been obtained for NI and TEM, which comfort the results on the impact of hydrogen on the different dislocation structures.

From this study, the origin of the softening and hardening effects of hydrogen is still not characterised. Therefore, further analysis should be performed at a lower length scale in order to evaluate the interaction between the different defects induced by the incorporation of hydrogen and by fatigue. Furthermore, the evolution of the back stress depending on the different hydrogen concentration is still not explained and will be investigated in the second part of the companion work.

References

Akiyama, E., Li, S., 2016. Electrochemical hydrogen permeation tests under galvanostatic hydrogen charging conditions conventionally used for hydrogen embrittlement study. Corros. Rev. 34. https://doi.org/10.1515/corrrev-2015-0049

Amelinckx, S., 1971. The direct observation of dislocations, 3. printing. ed, Solid state physics, Acad. Press, New York.

Argon, A.S., 1996. Mechanical properties of single-phase crystalline media: Deformation at low temperatures, in: Physical Metallurgy. Elsevier, pp. 1877–1955.

Ashby, M.F., Hirth, J.P., 1986. Perspectives in hydrogen in metals.

Barnoush, A., 2008. Hydrogen embrittlement, revisited by in situ electrochemical nanoindentation. Universität des Saarlandes.

Barnoush, A., Vehoff, H., 2010. Recent developments in the study of hydrogen embrittlement: Hydrogen effect on dislocation nucleation. Acta Mater. 58, 5274–5285. https://doi.org/10.1016/j.actamat.2010.05.057

Barnoush, A., Vehoff, H., 2008. In situ electrochemical nanoindentation: A technique for local examination of hydrogen embrittlement. Corros. Sci. 50, 259–267. https://doi.org/10.1016/j.corsci.2007.05.026

Beachem, C.D., 1972. A new model for hydrogen-assisted cracking (hydrogen “embrittlement”). Metall. Mater. Trans. B 3, 441–455. https://doi.org/10.1007/BF02642048

Birnbaum, H.K., Sofronis, P., 1994. Hydrogen-enhanced localized plasticity—a mechanism for hydrogen-related fracture. Mater. Sci. Eng. A 176, 191–202. https://doi.org/10.1016/0921-5093(94)90975-X

Blanc, C., Aubert, I., 2019. Mechanics - Microstructure - Corrosion Coupling. Elsevier Publisher.

Boniszewski, T., Smith, G.C., 1963. The influence of hydrogen on the plastic deformation ductility, and fracture of nickel in tension. Acta Metall. 11, 165–178. https://doi.org/10.1016/0001-6160(63)90209-8

Bouteau, G., 2013. Etude de la microstructure et de la concentration de lacunes dans le nickel monocristallin déformé en fatigue (Master Thesis). Université de La Rochelle, Laboratoire des Sciences de l’Ingénieur pour l’Environnement.

Buque, C., 2001. Dislocation structures and cyclic behaviour of [011] and [-111]-oriented nickel single crystals. Int. J. Fatigue 23, 671–678. https://doi.org/10.1016/S0142-1123(01)00032-9

Carr, N.Z., McLellan, R.B., 2004. The thermodynamic and kinetic behavior of metal–vacancy–hydrogen systems. Acta Mater. 52, 3273–3293. https://doi.org/10.1016/j.actamat.2004.03.024

Castelluccio, G.M., Geller, C.B., McDowell, D.L., 2018. A rationale for modeling hydrogen effects on plastic deformation across scales in FCC metals. Int. J. Plast. 111, 72–84. https://doi.org/10.1016/j.ijplas.2018.07.009

Delafosse, D., 2012. Hydrogen effects on the plasticity of face centred cubic (fcc) crystals, in: Gaseous Hydrogen Embrittlement of Materials in Energy Technologies. Elsevier, pp. 247–285. https://doi.org/10.1533/9780857095374.2.247

Delafosse, D., Magnin, T., 2001. Hydrogen induced plasticity in stress corrosion cracking of engineering systems. Eng. Fract. Mech. 68, 693–729. https://doi.org/10.1016/S0013-7944(00)00121-1

Dickson, J.I., Boutin, J., Handfield, L., 1984. A comparison of two simple methods for measuring cyclic internal and effective stresses. Mater. Sci. Eng. 64, L7–L11. https://doi.org/10.1016/0025-5416(84)90083-1

Dickson, J.I., Handfield, L., L'Esperance, G., 1983. Cyclic softening and thermally activated deformation of titanium and zirconium. Mater. Sci. Eng. 60, L3–L7. https://doi.org/10.1016/0025-5416(83)90190-8

dos Santos, D.S., Tavares, S.S.M., Miraglia, S., Fruchart, D., dos Santos, D.R., 2003. Analysis of the nanopores produced in nickel and palladium by high hydrogen pressure. J. Alloys Compd. 356–357, 258–262. https://doi.org/10.1016/S0925-8388(03)00170-1

Eastman, J., Heubaum, F., Matsumoto, T., Birnbaum, H.K., 1982. The effect of hydrogen on the solid solution strengthening and softening of nickel 8.

Ebenstein, D.M., Wahl, K.J., 2006. A comparison of JKR-based methods to analyze quasi-static and dynamic indentation force curves. J. Colloid Interface Sci. 298, 652–662. https://doi.org/10.1016/j.jcis.2005.12.062

Feaugas, X., 2003. Tensile and cyclic hardening: Back and effective stresses concepts and their applications. Recent Res. Mater. Sci. 4, 35–64.

Feaugas, X., 1999. On the origin of the tensile flow stress in the stainless steel AISI 316L at 300 K: back stress and effective stress. Acta Mater. 47, 3617–3632. https://doi.org/10.1016/S1359-6454(99)00222-0

Feaugas, X., Delafosse, D., 2019. Chapter 9: Hydrogen and Crystal Defects Interactions: Effects on Plasticity and Fracture, in: Mechanics - Microstructure - Corrosion Coupling. Elsevier Publisher, pp. 199–222.

Feaugas, X., Haddou, H., 2007. Effects of grain size on dislocation organization and internal stresses developed under tensile loading in fcc metals. Philos. Mag. 87, 989–1018. https://doi.org/10.1080/14786430601019441

Feaugas, X., Pilvin, P., 2009. A Polycrystalline Approach to the Cyclic Behaviour of f.c.c. Alloys - Intra-Granular Heterogeneity. Adv. Eng. Mater. 11, 703–709. https://doi.org/10.1002/adem.200900039

Fischer-Cripps, A.C., 2007. Introduction to contact mechanics, Mechanical engineering. Springer New York.

Fukai, Y., 2005. The metal-hydrogen system: basic bulk properties, 2. ed, Materials Science. Springer, Berlin.

Gangloff, R.P., Somerday, B.P., 2011. Gaseous hydrogen embrittlement of materials in energy technologies, Woodhead Publisher. ed.

Gao, Y., Bei, H., 2016. Strength statistics of single crystals and metallic glasses under small stressed volumes. Prog. Mater. Sci. 82, 118–150. https://doi.org/10.1016/j.pmatsci.2016.05.002

Gentet, D., 2009. Compréhension et modélisation du comportement mécanique cyclique anisotherme de l'acier austénitique AISI 316L(N). Université de La Rochelle.

Ghermaoui, I.M.A., Madani, K., Oudriss, A., Feaugas, X., 2019. Plastic deformation of (001) nickel single crystal oriented for multi-slips: some effects of hydrogen solute. Sci. Rep. 9:13042 https://doi.org/10.1038/s41598-019-49420-6

Girardin, G., Delafosse, D., 2004. Measurement of the saturated dislocation pinning force in hydrogenated nickel and nickel base alloys. Scr. Mater. 51, 1177–1181. https://doi.org/10.1016/j.scriptamat.2004.07.012

Girardin, G., Huvier, C., Delafosse, D., Feaugas, X., 2015. Correlation between dislocation organization and slip bands: TEM and AFM investigations in hydrogen-containing nickel and nickel–chromium. Acta Mater. 91, 141–151. https://doi.org/10.1016/j.actamat.2015.03.016

Gu, Y., El-Awady, J.A., 2018. Quantifying the effect of hydrogen on dislocation dynamics: A three-dimensional discrete dislocation dynamics framework. J. Mech. Phys. Solids 112, 491–507. https://doi.org/10.1016/j.jmps.2018.01.006

Hachet, G., Metsue, A., Oudriss, A., Feaugas, X., 2018. Influence of hydrogen on the elastic properties of nickel single crystal: A numerical and experimental investigation. Acta Mater. 148, 280–288. https://doi.org/10.1016/j.actamat.2018.01.056

Hachet, G., Li, J., Hallil, M., Metsue, A., Oudriss, A., Bouhattate, J., Feaugas, X., 2019, A multi-scale analysis of the different interactions between defects and hydrogen: a review on the contribution of the elastic fields. Eng. Fract. Mech. 218, 106621. https://doi.org/10.1016/j.engfracmech.2019.106621

Hajilou, T., Deng, Y., Rogne, B.R., Kheradmand, N., Barnoush, A., 2017. In situ electrochemical microcantilever bending test: A new insight into hydrogen enhanced cracking. Scr. Mater. 132, 17–21. https://doi.org/10.1016/j.scriptamat.2017.01.019

Harris, Z.D., Lawrence, S.K., Medlin, D.L., Guetard, G., Burns, J.T., Somerday, B.P., 2018. Elucidating the contribution of mobile hydrogen-deformation interactions to hydrogen-induced intergranular cracking in polycrystalline nickel. Acta Mater. 158, 180–192. https://doi.org/10.1016/j.actamat.2018.07.043

Hertz, H., 1881. Ueber die Berührung festerelastischer Körper. J Für Reine Angew Math 92, 156–171. https://doi.org/10.1515/crll.1882.92.156

Hirth, J.P., 1980. Effects of hydrogen on the properties of iron and steel. Metall. Trans. A 11, 861–890. https://doi.org/10.1007/BF02654700

Hughes, D.A., Hansen, N., 2000. Microstructure and strength of nickel at large strains. Acta Mater. 48, 2985–3004. https://doi.org/10.1016/S1359-6454(00)00082-3

Kassner, M.E., Geantil, P., Levine, L.E., 2013. Long range internal stresses in single-phase crystalline materials. Int. J. Plast. 45, 44–60. https://doi.org/10.1016/j.ijplas.2012.10.003

Kimura, A., Birnbaum, H.K., 1987. The effects of cathodically charged hydrogen on the flow stress of nickel and nickel-carbon alloys. Acta Metall. 35, 1077–1088. https://doi.org/10.1016/0001-6160(87)90055-1

Kirchheim, R., 2007a. Reducing grain boundary, dislocation line and vacancy formation energies by solute segregation. II. Experimental evidence and consequences. Acta Mater. 55, 5139–5148. https://doi.org/10.1016/j.actamat.2007.05.033

Kirchheim, R., 2007b. Reducing grain boundary, dislocation line and vacancy formation energies by solute segregation. I. Theoretical background. Acta Mater. 55, 5129–5138. https://doi.org/10.1016/j.actamat.2007.05.047

Kirchheim, R., Somerday, B., Sofronis, P., 2015. Chemomechanical effects on the separation of interfaces occurring during fracture with emphasis on the hydrogen-iron and hydrogen-nickel system. Acta Mater. 99, 87–98. https://doi.org/10.1016/j.actamat.2015.07.057

Laird, C., 1996. Fatigue, in: Physical Metallurgy. Elsevier, pp. 2293–2397.

Lawrence, S.K., Yagodzinskyy, Y., Hänninen, H., Korhonen, E., Tuomisto, F., Harris, Z.D., Somerday, B.P., 2017. Effects of grain size and deformation temperature on hydrogen-enhanced vacancy formation in Ni alloys. Acta Mater. 128, 218–226. https://doi.org/10.1016/j.actamat.2017.02.016

Lee, K.A., McLellan, R.B., 1984. The diffusivity of hydrogen in nickel at low temperatures 3.

Li, J., Oudriss, A., Metsue, A., Bouhattate, J., Feaugas, X., 2017. Anisotropy of hydrogen diffusion in nickel single crystals: the effects of self-stress and hydrogen concentration on diffusion. Sci. Rep. 7. https://doi.org/10.1038/srep45041

Li, P., Li, S.X., Wang, Z.G., Zhang, Z.F., 2011. Fundamental factors on formation mechanism of dislocation arrangements in cyclically deformed fcc single crystals. Prog. Mater. Sci. 56, 328–377. https://doi.org/10.1016/j.pmatsci.2010.12.001

Li, P., Zhang, Z.F., Li, X.W., Li, S.X., Wang, Z.G., 2009. Effect of orientation on the cyclic deformation behavior of silver single crystals: Comparison with the behavior of copper and nickel single crystals. Acta Mater. 57, 4845–4854. https://doi.org/10.1016/j.actamat.2009.06.048

Li, T.L., Gao, Y.F., Bei, H., George, E.P., 2011. Indentation Schmid factor and orientation dependence of nanoindentation pop-in behavior of NiAl single crystals. J. Mech. Phys. Solids 59, 1147–1162. https://doi.org/10.1016/j.jmps.2011.04.003
Lynch, S.P., 2019. Discussion of some recent literature on hydrogen-embrittlement mechanisms: addressing common misunderstandings. Corros. Rev. Accepted.
Lynch, S.P., 2011. Mechanistic and fractographic aspects of stress-corrosion cracking (SCC), in: Stress Corrosion Cracking. Elsevier, pp. 3–89. https://doi.org/10.1533/9780857093769.1.3
Lynch, S.P., 1979. Hydrogen embrittlement and liquid-metal embrittlement in nickel single crystals. Scr. Metall. 13, 1051–1056.
Magnin, T., 1995. Chapter 5: SCC and CF Modellings Based on Corrosion-Deformation Interactions, in: Materials Science Forum. pp. 95–132.
Magnin, T., Bosch, C., Wolski, K., Delafosse, D., 2001. Cyclic plastic deformation behaviour of Ni single crystals oriented for single slip as a function of hydrogen content. Mater. Sci. Eng. A 314, 7–11. https://doi.org/10.1016/S0921-5093(00)01920-1
Martin, M.L., Dadfarnia, M., Nagao, A., Wang, S., Sofronis, P., 2019. Enumeration of the hydrogen-enhanced localized plasticity mechanism for hydrogen embrittlement in structural materials. Acta Mater. 165, 734–750. https://doi.org/10.1016/j.actamat.2018.12.014
McInteer, W.A., Thompson, A.W., Bernstein, I.M., 1980. The effect of hydrogen on the slip character of nickel. Acta Metall. 28, 887–894. https://doi.org/10.1016/0001-6160(80)90105-4
Miyata, K., 2003. Effect of hydrogen charging on dislocation behavior in Ni-Cr and Ni2Cr alloys. Metall. Mater. Trans. A 34, 1249–1257. https://doi.org/10.1007/s11661-003-0235-5
Mughrabi, H., 1988. Dislocation clustering and long-range internal stresses in monotonically and cyclically deformed metal crystals. Rev. Phys. Appliquée 23, 367–379. https://doi.org/10.1051/rphysap:01988002304036700
Mughrabi, H., 1987. The long-range internal stress field in the dislocation wall structure of persistent slip bands. Phys. Status Solidi A 104, 107–120. https://doi.org/10.1002/pssa.2211040108
Mughrabi, H., 1983. Dislocation wall and cell structures and long-range internal stresses in deformed metal crystals. Acta Metall. 31, 1367–1379.
Mughrabi, H., 1978. The cyclic hardening and saturation behaviour of copper single crystals. Mater. Sci. Eng. 33, 207–223. https://doi.org/10.1016/0025-5416(78)90174-X
Mughrabi, H., Ungár, T., Kienle, W., Wilkens, M., 1986. Long-range internal stresses and asymmetric X-ray line-broadening in tensile-deformed [001]-orientated copper single crystals. Philos. Mag. A 53, 793–813. https://doi.org/10.1080/01418618608245293
Nagumo, M., 2016. Fundamentals of hydrogen embrittlement. Springer Singapore.
Oliver, W.C., Pharr, G.M., 1992. An improved technique for determining hardness and elastic modulus using load and displacement sensing indentation experiments. J. Mater. Res. 7, 1564–1583. https://doi.org/10.1557/JMR.1992.1564
Oriani, R.A., 1970. The diffusion and trapping of hydrogen in steel. Acta Metall. 18, 147–157.
Oudriss, A., 2012. Influence des hétérogénéités métallurgiques sur les processus de diffusion et de piégeage de l'hydrogène dans le nickel. Université de La Rochelle.
Oudriss, A., Creus, J., Bouhattate, J., Conforto, E., Berziou, C., Savall, C., Feaugas, X., 2012. Grain size and grain-boundary effects on diffusion and trapping of hydrogen in pure nickel. Acta Mater. 60, 6814–6828. https://doi.org/10.1016/j.actamat.2012.09.004
Oudriss, A., Feaugas, X., 2016. Length scales and scaling laws for dislocation cells developed during monotonic deformation of (001) nickel single crystal. Int. J. Plast. 78, 187–202. https://doi.org/10.1016/j.ijplas.2015.11.003
Pedersen, O.B., 1990. Overview no. 89 Mechanism maps for cyclic plasticity and fatigue of single phase materials. Acta Metall. Mater. 38, 1221–1239. https://doi.org/10.1016/0956-7151(90)90194-L

Renner, E., Gaillard, Y., Richard, F., Amiot, F., Delobelle, P., 2016. Sensitivity of the residual topography to single crystal plasticity parameters in Berkovich nanoindentation on FCC nickel. Int. J. Plast. 77, 118–140. https://doi.org/10.1016/j.ijplas.2015.10.002

Roberston, I.M., Birnbaum, H.K., Sofronis, P., 2009. Chapter 91: Hydrogen effects on plasticity, in: Dislocations in Plasticity. Elsevier Amsterdam.

Robertson, I.M., Sofronis, P., Nagao, A., Martin, M.L., Wang, S., Gross, D.W., Nygren, K.E., 2015. Hydrogen Embrittlement Understood. Metall. Mater. Trans. B 46, 1085–1103. https://doi.org/10.1007/s11663-015-0325-y

Schmid, E., Boas, W., 1950. Plasticity of Crystals, London: Chapman & Hall. ed.

Sirois, E., Birnbaum, H.K., 1992. Effects of hydrogen and carbon on thermally activated deformation in nickel. Acta Metall. Mater. 40, 1977–1986.

Stenerud, G., Johnsen, R., Olsen, J.S., He, J., Barnoush, A., 2017. Effect of hydrogen on dislocation nucleation in alloy 718. Int. J. Hydrog. Energy 42, 15933–15942. https://doi.org/10.1016/j.ijhydene.2017.04.290

Troiano, A.R., 1960. The Role of Hydrogen and Other Interstitials in the Mechanical Behavior of Metals. Metallogr. Microstruct. Anal. 52, 54–60. https://doi.org/10.1007/s13632-016-0319-4

Underwood, E.E., 1973. Quantitative stereology for microstructural analysis, in: Microstructural Analysis: Tools and Techniques. Springer US, pp. 35–66.

Vlassak, J.J., Nix, W.D., 1994. Measuring the elastic properties of anisotropic materials by means of indentation experiments. J. Mech. Phys. Solids 42, 1223–1245. https://doi.org/10.1016/0022-5096(94)90033-7

Wan, D., Alvaro, A., Olden, V., Barnoush, A., 2018. Hydrogen-assisted fatigue crack growth in ferritic steels – a fractographic study. MATEC Web Conf. 165, 03004. https://doi.org/10.1051/matecconf/201816503004

Wan, D., Barnoush, A., 2019. Plasticity in cryogenic brittle fracture of ferritic steels: Dislocation versus twinning. Mater. Sci. Eng. A 744, 335–339. https://doi.org/10.1016/j.msea.2018.12.038

Wang, S., Nagao, A., Edalati, K., Horita, Z., Robertson, I.M., 2017. Influence of hydrogen on dislocation self-organization in Ni. Acta Mater. 135, 96–102. https://doi.org/10.1016/j.actamat.2017.05.073

Wen, M., Fukuyama, S., Yokogawa, K., 2007. Cross-slip process in fcc nickel with hydrogen in a stacking fault: An atomistic study using the embedded-atom method. Phys. Rev. B 75. https://doi.org/10.1103/PhysRevB.75.144110

Wilcox, B.A., Smith, G.C., 1964. The Portevin-Le Chatelier effect in hydrogen charged nickel. Acta Metall. 12, 371–376.

Windle, A.H., Smith, G.C., 1968. The Effect of Hydrogen on the Plastic Deformation of Nickel Single Crystals. Met. Sci. J. 2, 187–191. https://doi.org/10.1179/030634568790443314

Zhou, X., Ouyang, B., Curtin, W.A., Song, J., 2016. Atomistic investigation of the influence of hydrogen on dislocation nucleation during nanoindentation in Ni and Pd. Acta Mater. 116, 364–369. https://doi.org/10.1016/j.actamat.2016.06.061